JOURNAL OF SPACECRAFT AND ROCKETS
Vol. 34, No. 3, May–June 1997

Predicted Optical Characteristics of Solid Rocket Motor Exhaust in the Stratosphere

Edward J. Beiting*
The Aerospace Corporation, El Segundo, California 90245

Optical characteristics of large solid rocket motor exhaust in the stratosphere are predicted for portions of the near-ultraviolet, visible, and near-infrared spectral regions. Mie scattering calculations show that attenuation by the alumina particles is caused principally by the large-particle mode of the trimodal particle size distribution. The local attenuation in the plume as a function of wavelength and the transplume total attenuation due to particles as a function of time are predicted for several wavelengths. An expression for the total surface area of the particles is derived in terms of known parameters and the Sauter mean diameter. Mie theory is then used to show that this Sauter mean diameter can be measured using a two-color transmissometer. The absorption spectra due to the chemical constituents are predicted for the 200–400-nm wavelength interval for several times after vehicle passage. It is predicted that these absorptions are comparable to the attenuations due to particle scattering.

Nomenclature

A_p = cross-sectional area of plume, m^2
a = geometrical cross-sectional area of particle, cm^2
a_{tot} = total surface area of all particle per unit volume of air, $\mu m^2\ cm^{-3}$
C_m = mass of particles per unit volume of air, $g\ cm^{-3}$
D = particle diameter, μm
D_{max} = maximum measured particle diameter in a size distribution mode, μm
D_{min} = minimum measured particle diameter in a size distribution mode, μm
D_{32} = Sauter mean diameter of particle, μm
L = path length through a plume, m
l = light path coordinate through a plume, m
M_L = total mass of alumina exhausted from solid rocket motor per vehicle track length, $g\ m^{-1}$
$n_D(D)$ = particle number density with respect to particle diameter, $cm^{-3}\ \mu m^{-1}$
$n_j^{gas}(t)$ = concentration of molecular species j, cm^{-3}
$p + iq$ = complex index of refraction
Q = light scattering efficiency
$\bar{Q}$ = light scattering efficiency averaged over particle size distribution
r = radial coordinate in plume, m
T = transmission of light beam
t = time, s
v_{tot} = total volume of particles per unit mass of air, $\mu m^3\ cm^{-3}$
w = particle size distribution width, μm
α = Mie scattering particle size parameter, $\pi D/\lambda$
β_{av} = average total attenuation coefficient, cm^{-1}
β_{gas} = attenuation coefficient due to molecular absorption, cm^{-1}
$\beta_{particle}$ = attenuation coefficient due to particles, cm^{-1}
γ_i = particle mode parameter, μm^{-1}
θ = angle between light beam and plume axis
κ = attenuation parameter, $g^{-1}\ cm^2$
λ = wavelength of light, μm
$\rho(D)$ = mass density of alumina particles, $g\ cm^{-3}$
ρ_{av} = mass density averaged over size distribution, $g\ cm^{-3}$
σ = absorption cross section of a chemical species, cm^2

Received June 20, 1996; revision received Feb. 18, 1997; accepted for publication Feb. 19, 1997.

*Research Scientist, P.O. Box 92957, Los Angeles, CA 90009-2957. Member AIAA.

Introduction

In a companion paper, a model was developed for the characteristics of alumina (Al_2O_3) particles of solid rocket motor (SRM) exhaust in the stratosphere.[1] The motivation for that work was to further understand the local (<100 km in extent) effects of SRM exhaust on the Earth's ozone layer. Of particular interest is the verification of the fluid-mechanical–chemical-kinetic models that predict the creation of a transient ozone hole. Many of the verification techniques are optical and require an a priori knowledge of the optical absorption of the plume. Here, this model for the specific particle density and a model for SRM plume chemistry[2] are used to calculate the optical attenuation caused by the particles and the chemical constituents of the plume. The predictions are made for a Titan IV plume at an altitude of 20 km. Two wavelength intervals are considered: the near ultraviolet, where the chemical species have continuous absorption bands, and the near infrared, where the attenuation due to particles predominate. We do not consider discrete molecular transitions in the infrared. The results are useful for predicting the feasibility of measurements by in situ ultraviolet absorption spectrometers, infrared transmissometers, ground-based LIDAR[3] instruments, and existing instruments that use scattering sunlight for inferring chemical concentrations, i.e., Total Ozone Mapping Spectrometer[4] and High-Resolution Ozone Imager.[5] In addition, it is shown how transmission measurements at two infrared wavelengths can be used to indicate the total surface area of the particles available for heterogeneous chemical reactions.

The transmission of light through an inhomogeneous medium of particles and gas as a function of wavelength, time, and traversal length is

$$T(\lambda, t, L) = \exp\left\{-\int_0^L [\beta_{particle}(\lambda, t, l) + \beta_{gas}(\lambda, t, l)]\, dl\right\} \quad (1)$$

For a collection of identical spherical particles, the attenuation coefficient due to scattering can be written as the product of the scattering efficiency, the geometrical cross section of the particle, and the number density of particles:

$$\beta_{particle}(\lambda, t, l) = Q(D, \lambda)a(D)n[t, r(l)] \quad (2)$$

The scattering efficiency Q can be calculated rigorously as a function of particle diameter and wavelength using electromagnetic theory. (Note: The alumina exits the rocket combustion chamber as liquid droplets and cools rapidly to form spherical particles.[1]) The absorption coefficient due to the gas can be written as a product of the concentration and the absorption cross section of the individual species:

$$\beta_{gas}(\lambda, t, l) = \sum_j n_j^{gas}[t, r(l)]\sigma_j(\lambda) \quad (3)$$

In the following sections, we calculate the attenuation and absorption coefficients employing the chemical and particle models for the gas and particle densities.

Ultraviolet Attenuation

First consider the attenuation due to particles. If the particles are not of uniform size (polydisperse systems) but are of a single size-distribution mode, the attenuation coefficient in Eq. (2) can be generalized and written in terms of mean values[6]:

$$\beta_{\text{particle}}(\lambda, t, l) = \frac{3\bar{Q}(D_{32}, w, p + iq, \lambda)C_m[t, r(l)]}{2\rho_{\text{av}} D_{32}} \tag{4}$$

C_m is the mass concentration of the particles in the medium (g cm^{-3} of air) given by

$$C_m(r, t) = \int_{D_{\min}}^{D_{\max}} n_D(D, r, t)\rho(D)V(D)\,\mathrm{d}D \tag{5}$$

The average mass density for the particles in the mode, ρ_{av}, is calculated using

$$\rho_{\text{av}} \equiv \frac{\int_{D_{\min}}^{D_{\max}} n_D(D)\rho(D)\,\mathrm{d}D}{\int_{D_{\min}}^{D_{\max}} n_D(D)\,\mathrm{d}D} \tag{6}$$

where the particle mass density as a function of its diameter can be written[1]

$$\rho(D) = 1.65 + 2.4 \times 10^{-0.195D} \qquad (D \text{ in } \mu\text{m}, \rho \text{ in g/cm}^3) \tag{7}$$

D_{32} is the volume-weighted-to-area-weighted (Sauter) mean diameter

$$D_{32} \equiv \frac{\int_{D_{\min}}^{D_{\max}} n_D(D)D^3\,\mathrm{d}D}{\int_{D_{\min}}^{D_{\max}} n_D(D)D^2\,\mathrm{d}D} \tag{8}$$

and $\bar{Q}$ is the efficiency averaged over the particle distribution function:

$$\bar{Q} = \frac{\int_{D_{\min}}^{D_{\max}} n_D(D)Q[\alpha(D), p + iq]D^2\,\mathrm{d}D}{\int_{D_{\min}}^{D_{\max}} n_D(D)D^2\,\mathrm{d}D} \tag{9}$$

The particle size distribution is given by[1]

$$n_D(D, r, t) = \left(\frac{344}{t}\right)^2 \exp\left(-\frac{r}{1.75t}\right) \sum_{i=1}^{3} n_i e^{-\gamma_i D} \tag{10}$$

where t is in seconds, r is in meters, and the summation is over the three particle-size modes. The parameters required for these modes are given in Table 1. This model predicts the particle size distribution and density of plumes of a Titan IV vehicle in the 18–40-km range during its early expansion. Equation (4) is a useful formulation of scattering by a polydisperse system of particles because $\bar{Q}$ depends primarily on the Sauter mean diameter and is independent of the shape of the size distribution function for a monomodal distribution.[7] Furthermore, for the case of small absorption (small imaginary component of the index of refraction), the ratio $\bar{Q}(\lambda_1)/\bar{Q}(\lambda_2)$ is a monotonic function of D_{32} for $\lambda_1/3 < D_{32} < \lambda_2$, thus permitting the Sauter mean diameter to be determined by measuring the transmittance at only two wavelengths, as will be discussed.

Table 1 Particle-size mode parameters

Mode	n_i, m^{-3} μm^{-1}	γ_i, μm^{-1}	$D_{\min}$, μm	$D_{\max}$, μm	D_{32}, μm
Small	8.3×10^{12}	63.3	0.025	0.244	0.056
Medium	1.8×10^{8}	3.13	0.245	0.99	1.0
Large	3.3×10^{7}	0.80	1.0	10	3.6

Mie scattering theory is used to calculate the mean scattering efficiency. Mie theory is a rigorous application of Maxwell's equations to the problem of the scattering of electromagnetic waves by spheres of arbitrary size.[8,9] The results presented here were obtained using an extension of an existing Fortran code[10] that permits the calculation of the mean value of the scattering efficiency for a distribution of particle sizes. The code uses a lognormal distribution for the particle sizes, but, as noted above, the mean values of the scattering efficiency are insensitive to the shape of the distribution function. This is true only for monomodal particle size distributions and so does not strictly apply to this (trimodal) application. However, if the attenuation is negligible for all but one mode, then the distribution may be considered to be monomodal for the purposes of light scattering. This has been shown to be true for a large SRM plume at infrared wavelengths and nearly true at ultraviolet wavelengths.

Figure 1 shows calculated mean efficiencies as a function of the Sauter mean diameter for a monomodal lognormal dispersion distribution with a standard deviation of 1.5 and an assumed imaginary refractive index of zero. The assumption of small absorption is justified by previous studies.[11,12] Figure 1a uses a real refractive index of 1.8, which is characteristic of rocket plume alumina particles for wavelengths of 200, 300, and 400 nm. Figure 1b shows a similar calculation for wavelengths of 0.5, 2.75, and 5.0 μm. A real index of refraction of 1.7 is realistic for these wavelengths.[13] The scattering efficiency is greatest when the mean particle diameter is approximately equal to the wavelength of light. At much smaller diameters, the efficiency (the ratio of the scattering cross section to the geometrical cross section) approaches small values that can be calculated using Rayleigh theory, whereas at larger diameters the efficiency approaches a value of two. The mean scattering efficiencies

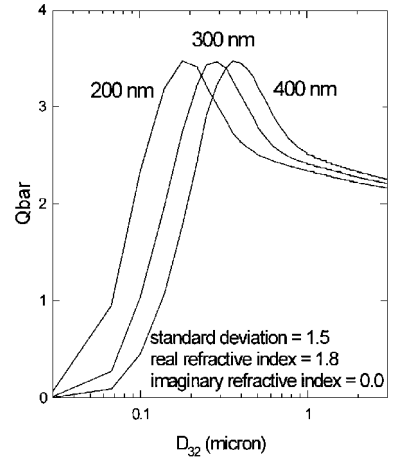

a) Near-ultraviolet

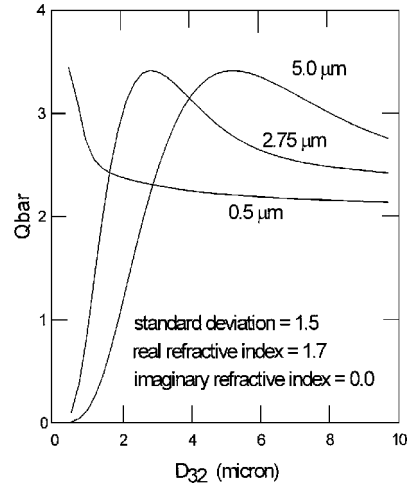

b) Visible and infrared wavelengths

Fig. 1 Calculated mean efficiency factors as a function of D_{32}.

Table 2 Particle scattering efficiencies and attenuation coefficients

Mode	D_{32}, μm	ρ, g/cm^3	C_m, g/cm^3	$\lambda = 0.2\,\mu$m $\bar{Q}$	$\lambda = 0.2\,\mu$m β_{av}, cm^{-1}	$\lambda = 0.3\,\mu$m $\bar{Q}$	$\lambda = 0.3\,\mu$m β_{av}, cm^{-1}	$\lambda = 0.4\,\mu$m $\bar{Q}$	$\lambda = 0.4\,\mu$m β_{av}, cm^{-1}	$\lambda = 0.5\,\mu$m $\bar{Q}$	$\lambda = 0.5\,\mu$m β_{av}, cm^{-1}	$\lambda = 1.0\,\mu$m $\bar{Q}$	$\lambda = 1.0\,\mu$m β_{av}, cm^{-1}	$\lambda = 5.0\,\mu$m $\bar{Q}$	$\lambda = 5.0\,\mu$m β_{av}, cm^{-1}
Small	0.056	4.0	3.0E−11	0.57	1.1E−6	0.14	2.8E−7	0.046	9.2E−8	0.015	3.0E−8	1.6E−5	3.2E−11	1.5E−6	3.0E−12
Medium	1.0	3.6	3.8E−11	2.35	3.7E−7	2.42	3.8E−7	2.52	3.9E−7	2.74	4.3E−7	0.9	1.4E−7	0.13	2.0E−8
Large	3.6	2.6	2.5E−9	2.15	8.6E−6	2.19	8.8E−6	2.22	8.9E−6	2.3	9.2E−6	2.9	1.2E−5	3.3	1.3E−5

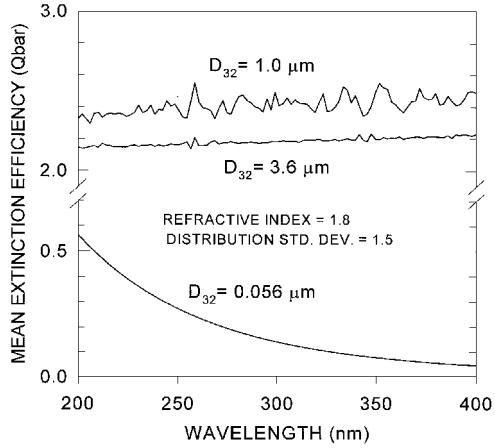

Fig. 2 Efficiency factors for three Sauter mean diameters corresponding to the measured size distributions of large SRM particles in the stratosphere as a function of wavelength.

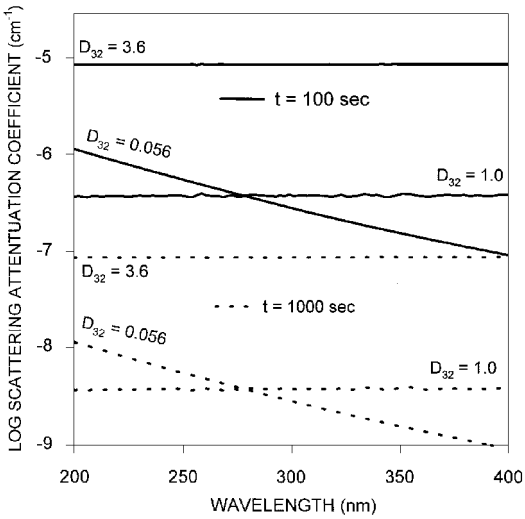

Fig. 3 Attenuation coefficients using the particle-plume model at times of 100 s (——) and 1000 s (- - - -) after SRM passage: scattering coefficient.

for selected wavelengths of interest for each of the three particle size modes expected in the plume are given in Table 2.

Figure 2 displays the mean scattering efficiencies as a function of wavelength in the 200–400-nm spectral region for the three Sauter mean diameters of the trimodal particle size distribution. The efficiency factors for the small particles ($D_{32} = 0.056\,\mu$m, bottom half of Fig. 2) are small for all wavelengths in this spectral range. The medium-particle ($D_{32} = 1.0\,\mu$m) and large-particle ($D_{32} = 3.6\,\mu$m) mode scattering efficiencies are significant at all of these wavelengths. The mean scattering cross section $\bar{Q}\bar{A}$ will be large for the large particles in this wavelength interval, but the number densities will favor the small-particle attenuation coefficients. The particle attenuation coefficient is calculated for each particle size mode using Eq. (4), where $\bar{Q}$ is taken from Fig. 2 and C_m is calculated for each mode using Eq. (5) and the particle distribution given by Eq. (10). The results for the spatially averaged values of the attenuation coefficient are shown in Fig. 3 and for selected wavelengths in Table 2. The coefficients were calculated for $t = 100$ and 1000 s after vehicle passage. The spatial average was calculated over a region between plume centerline and the radial position where the particle number density falls to e^{-2} times its peak (centerline) value. Using e^{-1} to define the averaging region increases the average attenuation coefficients by a factor of 1.4. The attenuation coefficients at plume centerline are 2.3 times those shown.

These curves indicate that the optical attenuation due to the large-mode particles in this spectral region is at least 8 times that due to the small- and medium-mode particles. The advantage of the large number density of the small-particle distribution is outweighed by the large scattering efficiencies and the large geometrical cross sections of the large particles. Thus for the purposes of optical measurements in this near-ultraviolet spectral interval, the particle size distribution may be approximated by a monomodal distribution, and inference of Sauter mean diameter from particle attenuation measurements at two or more wavelengths will correctly yield the D_{32} values for the large mode distribution. However, if this attenuation is comparable to the molecular absorbances, such an inference will be precluded.

Absorption Spectra

All of the expected chemical species of interest in a Titan SRM plume have significant absorption cross sections in the near-ultraviolet spectral region. This statement is also true for most of the ambient stratospheric species. This absorption may present the opportunity to monitor the concentration of these species with an absorption spectrograph. However, this spectral grouping also implies spectral congestion because the absorptions are broad and for the most part unstructured. Predicting the spectra relies on the ability to model the concentrations of the expected species and the availability of absolute absorption cross sections. Results from the current version of a model by Brady and Martin[2] will be used to calculate the chemical concentrations as a function of time after vehicle passage. Absolute absorption cross sections of most of the chemical species of interest have been measured at the ambient stratospheric temperature.

The model by Brady and Martin uses SURFACE CHEMKIN[14] and the output from the chemical-fluid dynamics model of the Titan IV SRM combustion due to Zittel[15] to calculate the species concentrations in the plume. The concentrations from the Brady–Martin model are calculated for a given stratospheric altitude and time, but this model does not predict spatial distributions. It does allow calculations of heterogeneous chemical reactions and the differentiation of isomers such as OClO and ClOO that have different absorption spectra. Using the latest measurement of surface reaction rate constants[16,17] and the calculated particle surface area from the model of the alumina particles, the model predicts that heterogeneous reactions will not be important. However, the concentrations are a sensitive function of the plume dispersion rate. This sensitivity is discussed in Appendix A. Information on the absolute absorption cross section can be found in Appendix B.

Figure 4 displays the expected absorption coefficients for the ambient species in the stratosphere at an altitude of 20 km between 200 and 400 nm. The concentrations used to generate these curves are also shown. The concentrations were calculated using the LNLL two-dimensional model of the troposphere and stratosphere as presented in Appendix 2 of Ref. 20. This version of the model represents a 1990 ambient atmosphere for March 15 at local noon and 40°N latitude. The composite curve is the expected spectrum and is dominated by O_3 with contributions due to O_2 and NO_2 in the short- and long-wavelength regions, respectively. (The short-wavelength discontinuity in the curve is an artifact caused by missing data for O_2 below 205 nm.) The accurate O_3 cross sections and constant O_3 density outside the plume at a given altitude can serve to calibrate

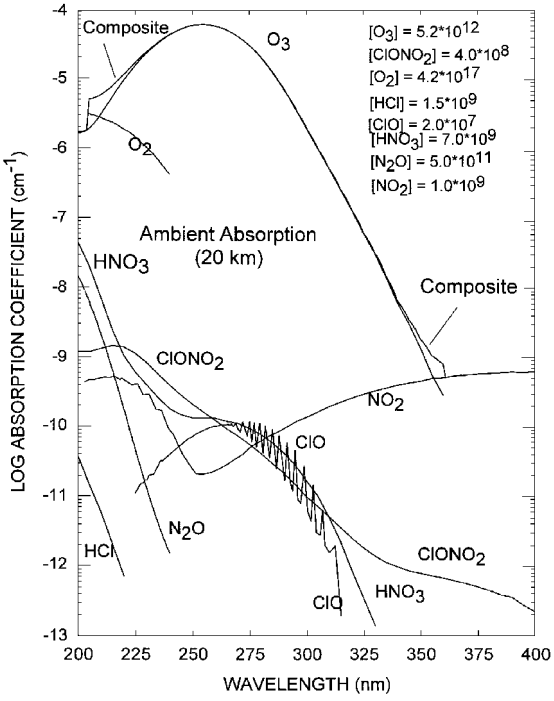

Fig. 4 Absorption coefficients of ambient stratospheric species and expected absorption spectrum (marked composite).

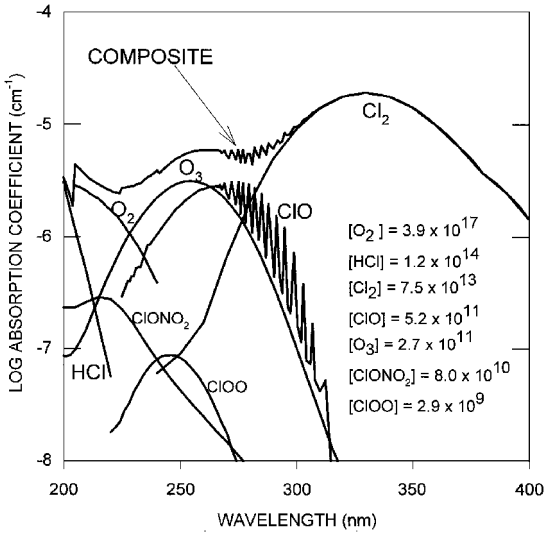

Fig. 5 Expected absorption coefficients and absorption spectrum in plume using predicted densities at 100 s after Titan IV passage.

an airborne absorption spectrograph over a five-order-of-magnitude dynamic range between passes through the plume.

Figure 5 illustrates the plume absorption coefficients 100 s after Titan IV passage. Here the spectrum shows contributions from HCl, O_2, O_3, ClO, and Cl_2. Because the kinetics model calculates an average density, the spectra will vary considerably between the centerline, where there will be greater contribution than shown from the chlorine species, and the plume edge, where the O_3 absorption will be more pronounced. The spectrum has changed to nearly that of the ambient atmosphere at 1000 s, as indicated in Fig. 6. Here only contributions from O_2, O_3, and Cl_2 are discernible. Figure 3 indicates that these spectra will compete with attenuation caused by light scattering by the particles. The constant attenuation due to the large-particle mode nearly equals that due to the gaseous chemical species at 100 s. This is also true for the attenuation due to the Cl_2 at 1000 s. Because the attenuation due to the particles is nearly constant in this spectral region, it may be possible to measure the relative concentrations of the aforementioned chemical species using an in situ absorption spectrograph. However, the measurement of the Sauter mean diameter by a transmissometer will be difficult due to the large overlying molecular absorption. This particle measurement is more readily made at infrared wavelengths, where the molecular absorption consists of narrow lines that are easily avoided.

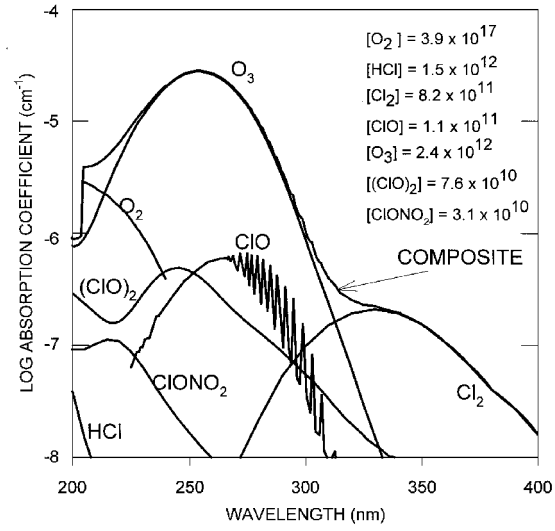

Fig. 6 Expected absorption coefficients and absorption spectrum in plume using predicted densities at 1000 s after Titan IV passage.

Applications

In this section, two applications of the particle model and the optical scattering results are considered. The first is a straightforward method of measuring the specific density of total particle surface area using a two-wavelength transmissometer. This parameter, together with the reactive sticking coefficient, can be used to discover the effect of heterogeneous chemical reactions in the plume. The second is the measurement of the transmission across the plume at an arbitrary angle. This information is useful for estimating the feasibility of plume measurements using LIDAR.

Measurement of Total Particle Surface Area Per Unit Air Volume

If all of the particles in the plume have the same size, the total surface area of the particles per unit gas volume is simply the total number of particles per unit volume times the surface area per particle. For a particle size distribution, the total particle surface area per unit gas volume is

$$a_{\text{tot}} = \pi \int_0^\infty n_D(D) D^2 \, \mathrm{d}D \tag{11}$$

Similarly, the total volume of particles per unit gas volume is

$$v_{\text{tot}} = \frac{\pi}{6} \int_0^\infty n_D(D) D^3 \, \mathrm{d}D \tag{12}$$

Now, we note that

$$a_{\text{tot}}/v_{\text{tot}} = 6/D_{32} \tag{13}$$

where Eq. (8) was used for D_{32}. Furthermore, we note that $v_{\text{tot}} = M_L/A_p\rho_{\text{av}}$. Substituting this expression for v_{tot} in Eq. (13), we obtain

$$a_{\text{tot}} = \frac{6M_L}{A_p \rho_{\text{av}} D_{32}} \tag{14}$$

Equation (14) is an important result because it shows how the volume density of the total particle surface area can be obtained from known or easily measured quantities. The mass of the alumina per vehicle track length is 15 g/cm for a Titan IV at 20 km, the cross-sectional area of the plume is measured on traversal of the plume, and the average density of the particles is approximately 3.0 g/cm^3. Now consider measuring the Sauter mean diameter by a two-color transmissometer.

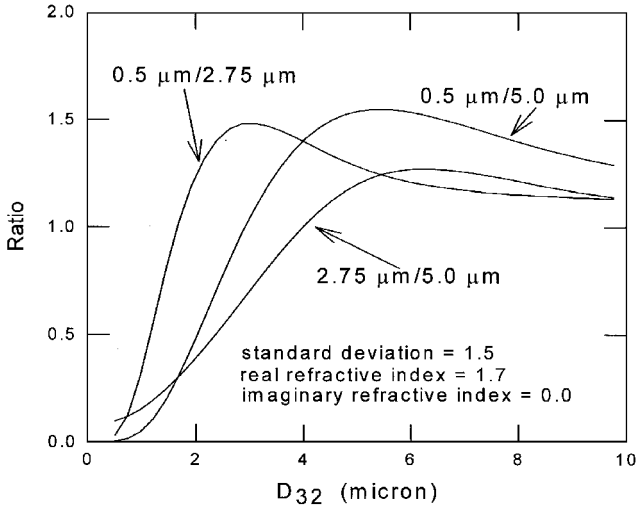

Fig. 7 Ratio of the mean scattering efficiencies [see Eq. (15)] for three wavelengths calculated using Mie theory. Locating the ratio of the logarithms of the measured transmission at two wavelengths on the ordinate of the function allows the Sauter mean diameter D_{32} to be inferred from the abscissa.

From Eqs. (1) and (4), the ratio of measurements of transmission at two wavelengths can be expressed as a simple function of the mean efficiency of a distribution with a given D_{32},

$$f(D_{32}) \equiv \frac{\overline{Q_2(D_{32})}}{\overline{Q_1(D_{32})}} = \frac{\ln T(\lambda_2)}{\ln T(\lambda_1)} \tag{15}$$

This function can be calculated for the wavelengths and refractive indices of the particles using Mie scattering theory. This was done for three wavelengths in the visible and infrared spectral regions where the attenuation is larger than in the ultraviolet region and the descrete molecular absorptions are narrow and easily avoided. The results are shown in Fig. 7. For the case of small absorption (small imaginary component of the index of refraction), this function is monotonic for $\lambda_1/3 < D_{32} < \lambda_2$. Accordingly, the value of D_{32} can be inferred from one of these curves given the measured transmissions for a monomodal distribution. From Table 2, the attenuation due to the large-particle distribution is orders of magnitude greater than that of the small- and medium-particle distributions at infrared wavelengths due to their geometrical size and scattering efficiencies. Thus the distribution will appear to be monomodal, and only the Sauter mean diameter of the large mode will be measured. Although the largest change in the function is given by the ratio $\bar{Q}(D_{32}, \lambda = 0.5\,\mu\text{m})/\bar{Q}(D_{32}, \lambda = 5.0\,\mu\text{m})$, the ratio $\bar{Q}(D_{32}, \lambda = 2.75\ \mu\text{m})/\bar{Q}(D_{32}, \lambda = 5.0\,\mu\text{m})$ is the better ratio to use for this application because the attenuation coefficient at 2.75 μm is somewhat greater for the large mode particles, the attenuation is smaller for the medium mode particles at 0.5 μm (better approximating a monomodal distribution), and the expected mean diameter lies near the center of the region of monotonicity.

Only one of the curves shown in Fig. 7 is required to measure D_{32} if the value of the width w of the distribution and the complex refractive index are known. If these quantities are not known, several transmission measurements can be taken at different wavelengths. The ratios of these measurements can then be compared with the calculated curves of ratios of $\bar{Q}(D_{32})$ vs D_{32}. If $\bar{Q}(D_{32})$ is calculated for the correct size distribution width and index of refraction, then all of the measured ratios will yield identical values of D_{32}. Alternatively, a multiparameter fit of the calculated values of $\bar{Q}(D_{32}, w, p+iq)$ to the measured ratios will allow the determination of D_{32}, w, and $p+iq$. In practice, the value of the imaginary part of the refractive index (q) is small for alumina particles at wavelengths below 6.5 μm and may be ignored, leaving only three parameters to fit. For example, Kim et al.[11] used transmissions at five wavelengths to determine the Sauter mean particle diameter (0.150 μm ± 8%), standard deviation [1.50 (±3%)], and real index of refraction [1.63 (±8%) for visible wavelengths] of the particles at the edge of a plume from a small solid-propellant motor. This technique will only measure the surface area of the large mode particles. If the particle size distribution given by Eq. (10) is correct, this mode accounts for about two-thirds of the total surface area.

Table 3 Plume transmissions at 45 deg

Mode	D_{32}, μm	Transmission $\lambda = 0.2\,\mu$m	$0.3\,\mu$m	$5.0\,\mu$m
Small	0.056	0.964	0.991	1.000
Medium	1.0	0.989	0.989	0.999
Large	3.6	0.761	0.757	0.657

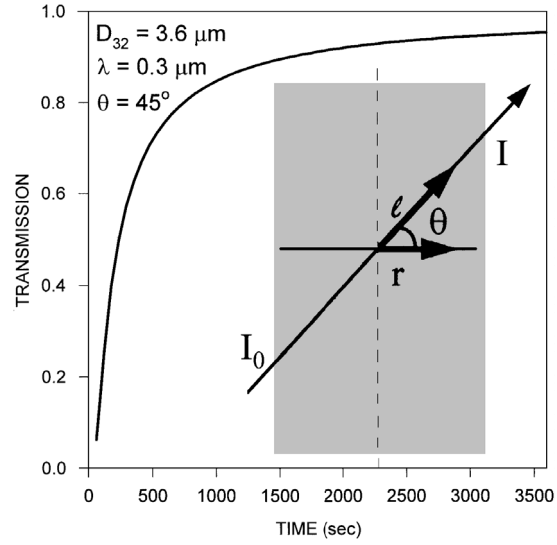

Fig. 8 Transmission of a beam of radiation across a Titan IV plume as a function of time after the passage of the SRM.

Light Transmission Across the Plume at an Arbitrary Angle

Here we consider the plume attenuation due to particles alone for a beam of light crossing the centerline of a plume and making an angle θ with respect to its axis (see Fig. 8). From Eqs. (1) and (4), the transmission is given by

$$T = \exp\left[-\kappa_i \int_{-r}^{r} C_m(r,t)\,\mathrm{d}r\right] \tag{16}$$

where the attenuation parameter is

$$\kappa_i = \frac{\overline{3Q_i(\lambda)}}{2\rho(D_{32i})D_{32i}\cos\theta} \tag{17}$$

i is the index for the particle size mode, and C_m is given by Eq. (5). Using the mean efficiencies from Table 2 and angle of 45 deg (an appropriate value, assuming a vertical LIDAR beam and a typical trajectory of a Titan IV in the stratosphere), transmissions through the plume at three wavelengths for each of the three particle modes are given in Table 3 at 10 min after SRM passage. Again, nearly all of the attenuation is due to the large particles. The time dependence of the transmission for the large mode particles at a wavelength of 300 nm (a typical LIDAR wavelength) is shown in Fig. 8. The plume becomes more than 50% transparent in the first 5 min. This result is consistent with initial stratospheric LIDAR measurements of a Titan IV plume but is the effect of the particle attenuation only. The measured attenuation would include the absorption due to molecular species. Differential attenuation, on and off molecular resonances, is easily accomplished in the infrared and permits the separation of the particle and chemical contributions.

Conclusions

The understanding of the interaction of a large SRM with the stratosphere can be significantly increased by measuring the properties of alumina particles and the concentration of chlorine species in the expanding plume as a function of time. Models that predict

significant quantities of active chlorine and local depressed ozone levels are sensitive to initial concentrations, reaction rate constants, total particle surface area, plume dispersion rate, etc., with nonlinear interlinking dependences. Data measuring the perturbations to the stratospheric chemistry by SRMs are nearly nonexistent. Optical techniques are a practical method to measure many of the required quantities, but the design of an appropriate optical instrument and the interpretation of the data require a priori information about the optical characteristic of the stratospheric plume. Information adequate for the design and application of such techniques was presented here. These studies indicate that nearly all of the scattering of light with wavelengths greater than 200 nm is due to the large-particle-size mode. At ultraviolet wavelengths, the absorption due to chemical species competes with the attenuation due to light scattering. The attenuation due to particles and gas-phase absorption decreases rapidly with time, making quantitative measurements difficult at times more than 20–30 min after vehicle passage. Any in situ instrument that relies on absorption will required a large dynamic range to monitor the species concentration from edge to centerline of the plume, as well as one or more multipass cells, with the longest having a path length of at least 1 km. Instruments that view attenuation across the entire plume should be readily feasible.

Appendix A: Chemical Concentration Sensitivity to Diffusion Parameters

The incorporation of the diffusion model into the chemical kinetics model of Brady and Martin[2] can be done several ways. We consider two methods, each of which requires choosing two initial parameters. The predicted species concentrations and persistence of the ozone hole are sensitive to these choices.

The functional form for the diffusion of the number density in the plume is[1]

$$n(r,t) = n_0(t_0/t)^2 \exp\{-(1/b)[(r/t) - (r_0/t_0)]\} \qquad \text{(A1)}$$

where n_0 is the particle number density at r_0 and t_0 and the diffusion parameter $b = 1.75$ m/s. The Brady–Martin model is one dimensional, assuming a constant concentration in a plume radius, and this concentration decreases through a dilution factor given by

$$\frac{1}{n}\frac{\partial n}{\partial t} = -\left(\frac{2}{t} - \frac{R_0}{bt^2}\right) \qquad \text{(A2)}$$

For an expanding plume, $t > R_0/2b$, and the time axis must be redefined, i.e., $t \rightarrow t - R_0/2b + t_0$, where t_0 is the starting time for the model, at which the concentration is n_0 and the radius is R_0. The Brady–Martin model predicts chemical concentrations based on initial concentrations and temperature calculated by Zittel's chemical–fluid-mechanical model,[15] which follows the combustion of Titan IV SRM from combustion chamber to 2 s after the exhaust exits the nozzle. The Brady–Martin model begins its calculation at 2 s when the radius of the plume is about 25 m. We assume these values for t_0 and R_0 in this first approach.

An alternative approach is to define a radius of the plume for the one-dimensional Brady–Martin model using the relation $n(R,t)/n(R_i,t) = e^{-A}$, so $R(t) = R_0 + Abt$. If $A = 1$ (or 2), the edge is defined as the radius where the density falls to e^{-1} (or e^{-2}) of its centerline density. Assuming the plume expands in the two dimensions normal to its axis, the dilution factor for this approach is

$$\frac{1}{n}\frac{\partial n}{\partial t} = \frac{-2A}{R_0 + Abt} \qquad \text{(A3)}$$

The concentrations of a nonreacting species (He) and O_3 are calculated using the Brady–Martin model for a Titan IV rocket at an altitude of 20 km for these two dilution factors. The results are shown in Fig. A1. The concentrations of the nonreacting helium show the purely dispersive effects. The solid lines show the helium and ozone concentration profiles generated when the model employed the dispersion parameters that were used to calculate the spectra shown in Figs. 6 and 7. The first approach shows a deeper ozone hole than the second and is not sensitive to a change of t_0 from 0 to 2 s for times greater than 10 s. The second approach is sensitive to the definition of the radius parameter A. Which approach and parameters give the most realistic concentrations can only be answered by measurements. The only known in situ measurement of O_3 concentration in an Titan III-C plume found a 40% decrease from ambient value about 12 min after vehicle passage at an altitude of 18 km.[18] (Note: A U.S. Air Force Program using LIDAR and in situ sampling in the stratosphere is currently collecting data to study this topic.) If this value is correct, the second approach (with a radius parameter between 1 and 2) is the more accurate. For both approaches, the ozone hole does not persist longer than about 1.5 h. This fast ozone recovery does not occur for a dilution factor based on the dispersion model of Watson et al.[19] For that case, the ozone hole persists for many hours, as shown by the bottom curve in Fig. A1. The concentrations used for calculating the absorption spectra shown in Figs. 5 and 6 were obtained using the dilution factor calculated using the second approach and a radius parameter of 1. The helium and ozone concentrations for this case are shown by the solid curves in Fig. A1.

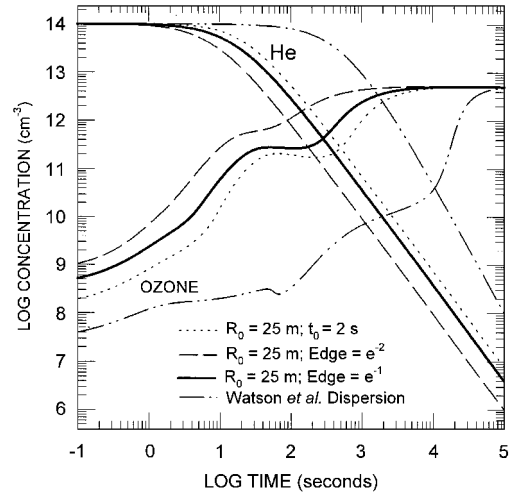

Fig. A1 Ozone and He concentrations in a Titan IV plume predicted by the Brady–Martin model using different dispersion characteristics.

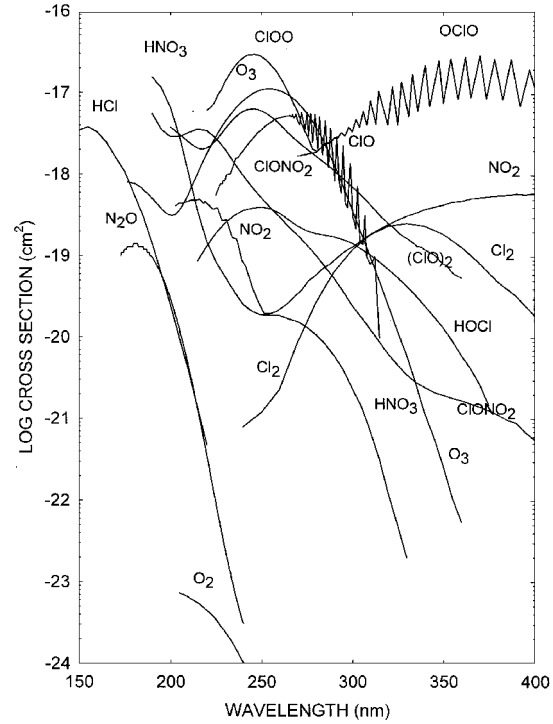

Fig. B1 Absolute absorption cross sections of stratospheric and SRM afterburning species.

Appendix B: Absolute Absorption Cross Sections

Data on the absolute absorption cross section exist for all of the relevant species in this work. The cross sections used to calculate the

absorption coefficients shown in Figs. 4–6 are presented in Fig. B1. Most of the data were taken from Jet Propulsion Laboratory (JPL) Publication 92-20 (Ref. 20), which compiles chemical kinetics and photochemical data for use in stratospheric modeling. The OClO data are from Ref. 21. The temperatures of the spectra shown are as follows: O_3 and NO_3, 273 K; N_2O, 215 K; HNO_3, 298 K; OClO, 293 K; and $(ClO)_2$, 225 K. Other temperatures were not listed in the JPL publication and are presumably room temperature. The models predict large concentrations of water vapor in the plume, and some species could be hydrolyzed. This can change the position and appearance of several of the spectra shown. For example, nearly all the structure of OClO is smoothed out when OClO is in water solution.[22] Thus there could be variations in the structure of species shown in Fig. B1, but they are probably not extensive, since the Brady–Martin model does allow water condensation and predicts virtually no liquid water.

Acknowledgments

This work was supported by the Environmental Management Division, USAF HQ SMC/CEV, and coordinated by the Environmental Programs Office of The Aerospace Corporation under Contract F04701-93-C-0094. The author thanks B. B. Brady for providing the chemical modeling results used to calculate the molecular absorption spectra. The author also thanks J. A. Gelbwachs for the 1996 personal communication of LIDAR measurements of a Titan IV plume. Useful conversations with J. A. Syage and L. R. Martin are gratefully acknowledged. The original Mie scattering source code was supplied by D. Netzer.

References

[1]Beiting, E. J., "Solid Rocket Motor Exhaust Model for Alumina Particles in the Stratosphere," *Journal of Spacecraft and Rockets*, Vol. 34, No. 3, 1997, pp. 303–310.

[2]Brady, B. B., and Martin, L. R., "Modeling Solid Rocket Booster Exhaust Plumes in the Stratosphere with SURFACE CHEMKIN," The Aerospace Corp., TR-95(5231)-9, El Segundo, CA, Sept. 1995.

[3]Dao, P., Gelbwachs, J. A., Farley, R., Garner, R., Soletsky, P., and Davidson, G., "LIDAR Stratospheric Solid Rocket Motor Exhaust Plume Measurements," AIAA Paper 97-0526, Jan. 1997.

[4]Syage, J. A., and Ross, M. N., "An Assessment of the Total Ozone Mapping Spectrometer for Measuring Ozone Levels in a Solid Rocket Plume," *Geophysical Research Letters*, Vol. 23, No. 22, 1996, pp. 3227–3230.

[5]McKenzie, D. L., Gutierrez, D. J., Hecht, J. H., Marbry, D. J., Ross, M. N., Tossano, G. S., Sivjee, M. G., and Stein, J. A., "System Requirements Review for the High-Resolution Ozone Imager (HIROIG)," The Aerospace Corp., TR-93(4231)-9, El Segundo, CA, Sept. 1993.

[6]Dobbins, R. A., Crocco, L., and Glassman, I., "Measurement of Mean Particle Sizes in Sprays from Diffractively Scattered Light," *AIAA Journal* Vol. 1, No. 8, 1963, pp. 1882–1886.

[7]Dobbins, R. A., and Jizmagian, G. S., "Optical Scattering Cross Sections for Polydispersions of Dielectric Spheres," *Journal of the Optical Society of America*, Vol. 56, No. 10, 1966, pp. 1345–1350.

[8]Van de Hulst, H. C., *Light Scattering by Small Particles*, Dover, New York, 1957, 1981.

[9]Kerker, M., *The Scattering of Light*, Academic, New York, 1969.

[10]Cashdollar, K. L., Lee, C. K., and Singer, J. M., "Three-Wavelength Light Transmission Technique to Measure Smoke Particle Size and Concentration," *Applied Optics*, Vol. 18, No. 11, 1979, pp. 1763–1769.

[11]Kim, H. O., Laredo, D., and Netzer, D. W., "Measurement of Submicrometer Al_2O_3 Particle in Plumes," *Applied Optics*, Vol. 32, No. 33, 1993, pp. 6834–6840.

[12]Nyquist, R. A., and Kagel, R. O., *Infrared Spectra of Inorganic Compounds (3800–45 cm^{-1})*, Academic, New York, 1971.

[13]Laredo, D., McCrorie II, J. C., Vaughn, J. K., and Netzer, C. W., "Motor and Plume Particle Size Measurements in Solid Propellant Micrometers," *Journal of Propulsion and Power*, Vol. 10, No. 3, 1994, pp. 410–418.

[14]Coltrin, M. E., Kee, R. J., and Rupley, F. M., "SURFACE CHEMKIN (Version 4.0): A Fortran Package for Analyzing Heterogeneous Chemical Kinetics at a Solid-Surface–Gas-Phase Interface," Sandia Corp., Rept. SAND90-8003B.UC-401, Sandia National Labs., Livermore, CA, 1991.

[15]Zittel, P. F., "Local Effects of Large, Solid Rocket Motors on Stratospheric Ozone," The Aerospace Corp., ATR-92(9558)-2, El Segundo, CA, Aug. 1992; also "Computer Model Predictions of the Local Effects of Large, Solid-Fuel Rocket Motors on Stratospheric Ozone," The Aerospace Corp., TR-94(4231)-9, El Segundo, CA, Sept. 1994.

[16]Lohn, P. D., Wong, E. Y., Molina, M. J., and Dension, M. R., "The Impact of Deorbiting Space Debris on Stratospheric Ozone," TRW, Engineering Rept. CDRL A005-2, El Segundo, CA, May 1994.

[17]Hanning-Lee, M. A., Brady, B. B., Martin, L. R., Syage, J. A., "Ozone Decomposition on Alumina: Implications for Solid Rocket Motor Exhaust," *Geophysical Research Letters*, Vol. 23, No. 15, 1996, pp. 1961–1964.

[18]Pergament, H. S., Gomberg, R. I., and Poppoff, I. G., "NO_x Deposition in the Stratosphere from the Space Shuttle Rocket Motors," NASA TM Z-58198, G-3, Jan. 1977, Appendix G.

[19]Watson, R. T., Smokler, P. E., and DeMore, W. B., "An Assessment of an F_2 or N_2O_4 Atmospheric Injection from an Aborted Space Shuttle Mission," Jet Propulsion Lab., Publication 77-81, California Inst. of Technology, Pasadena, CA, 1978.

[20]DeMore, W. B., Sander, S. P., Golden, D. M., Hampson, R. F., Kurylo, M. J., Howard, C. J., Ravishankara, A. R., Kolb, C. E., Molina, M. J., *Chemical Kinetics and Photochemical Data for Use in Stratospheric Modeling, Evaluation Number 10*, Jet Propulsion Lab., Publication 92-20, California Inst. of Technology, Pasadena, CA, 1992.

[21]Dunn, R. C., and Simon, J. D., "Excited State Photoreactions of Chlorine Dioxide in Water," *Journal of the American Chemical Society*, Vol. 114, No. 12, 1992, pp. 4856–4860.

[22]Dunn, R. C., Flanders, B. N., Vaida, V., and Simon, J. D., "The Spectroscopy of OClO in Polar Liquids," *Spectrochimica Acta*, Vol. 48A, No. 9, 1992, pp. 1293–1301.

I. D. Boyd
Associate Editor